QUT Digital Repository:
http://eprints.qut.edu.au/

Computationally Efficient Interference Detection in Videokeratoscopy Images

David Alonso-Caneiro, D. Robert Iskander, and Michael J. Collins

Contact Lens and Visual Optics Laboratory, School of Optometry, Queensland University of Technology
Victoria Park Road, Kelvin Grove Q4059, Australia
d.alonsocaneiro@qut.edu.au
{d.iskander,m.collins}@qut.edu.au

Abstract—An optimal videokeratoscopic image presents a strong well-oriented pattern over the majority of the measured corneal surface. In the presence of interference, arising from reflections from eyelashes or tear film instability, the pattern's flow is disturbed and the local orientation of the area of interference is no longer coherent with the global flow. Detecting and analysing videokeratoscopic pattern interference is important when assessing tear film surface quality, break-up time and location as well as designing tools that provide a more accurate static measurement of corneal topography. In this paper a set of algorithms for detecting interference patterns in videokeratoscopic images is presented. First a frequency approach is used to subtract the background information from the oriented structure and then a gradient-based analysis is used to obtain the pattern's orientation and coherence. The proposed techniques are compared to a previously reported method based on statistical block normalisation and Gabor filtering. The results indicate that the proposed technique leads, in most cases: to a better videokeratoscopic interference detection system, that for a given probability of the useful signal detection (99.7%) has a significantly lower probability of false alarm, and at the same time is computationally much more efficient than the previously reported method.

I. INTRODUCTION

Videokeratoscopy (or videokeratography) based on a Placido disk pattern is the current clinical standard to measure corneal surface topography. The pattern, consisting of a set of concentric rings, formed in a cone or bowl is projected on the anterior surface of the cornea and its reflection is imaged onto a CCD. Videokeratoscopy relies on a number of factors in order to get an accurate measure of the corneal surface topography. Minimal reflection from eyelashes, minimal eye movements, and good tear film quality are required to obtain an optimal reflected image [1], [2].

However, in practice, these optimal factors may not always be fulfilled, especially in situations where the subject presents poor tear film quality, nystagmus (uncontrolled eye-movement) or narrow palpebral aperture (distance between the eyelids). In such situations it is essential to detect the interference in the acquired videokeratoscopic image and separate it from the useful signal from which corneal topography can be estimated. Recently we have shown that separating these two factors improves the estimates of the corneal topography [3].

Dynamic videokeratoscopy techniques, which extend the traditional static corneal surface measurements, have been recently used to assess tear film surface quality [4], [5], [6],

[7]. The tear film is the outer thin layer of fluid that covers the cornea and the conjunctiva. This layer acts like a mirror and is responsible for reflecting the projected Placido disk ring pattern. A regular tear film surface, which is one of the key characteristics of a healthy tear film, produces an isotropic reflected pattern, while an irregular tear film produces an anisotropic reflected pattern. Hence an analysis of the pattern coherence is required to assess tear film surface quality [8].

Thus, it is necessary to detect interference patterns in videokeratoscopic images and separate the areas associated with them from the remaining areas that constitute the useful signal. The interference in an image can be seen as a disruption of the pattern's flow. An example of a videokeratoscopic image with interference from eyelashes and tear film instability that leads to ring fusion, indicated by the white arrow, is shown in Figure 1 (left).

We propose to use a Gaussian gradient-based algorithm [9] to detect interference patterns in videokeratoscopic images as a low computational approach to analyse oriented patterns. This approach will be compared to our previously reported technique based on a Gabor filter [3]. To evaluate the performance of the interference detection algorithm, we fit the pattern coherence data with a Gaussian mixture using an Expectation Maximisation algorithm, and estimate the probability of false alarm. In this paper we focus on detecting the useful signal from the videokeratoscopic image while the application of the interference separation and its location that could be used for tear film quality assessment is not considered here.

II. METHOLODOGY

When there is no interference, a videokeratoscopic image presents a relatively well-oriented pattern. In other words, all areas of the image within the corneal coverage have dominant local orientation. In order to evaluate this pattern and analyse its orientation we use a Gaussian gradient-based algorithm [9] that results in estimated local orientation angle and the degree of anisotropy or coherence. The coherence is a measurement of the consistency of the local orientation. If the Placido disk pattern is free of interference, the pattern would be perfectly isotropic whereas if there are disturbances in the local orientation flow, the pattern would became anisotropic. Therefore the coherence is an indicator of the interference in the image.
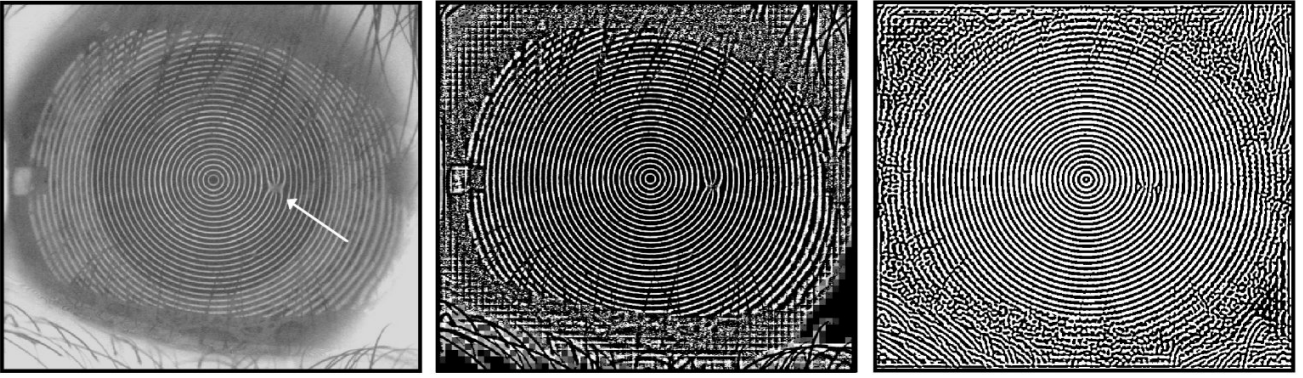
Fig. 1. An example of a videokeratoscopic image with reflections from upper and lower eyelashes and tear film instability (left) and its statistical block (centre) and frequency based (right) normalisations.

A. Background extraction

A videokeratoscopic image is composed of the image of the anterior eye masked by the reflected pattern of the Placido disk rings. The anterior eye image forms the background and does not provide any essential information for the analysis of the pattern. For that reason it is essential to remove the background in the videokeratoscopic image to avoid misleading information in further processing. This can be achieved with statistical block normalisation as used in [3], where an image was divided into small blocks in which the intensity information was normalised to zero-mean and unit variance.

An alternative normalisation can be achieved by noticing that the frequency content for the oriented pattern is located in a known narrow band because in most videokeratoscopic acquisitions the rings have semi-equidistant separation along the image, unless there is interference. Hence a frequency-based normalisation approach is proposed as a background subtraction.

A bandpass filter is used to filter the frequency content of the image that corresponds to Placido disk ring pattern. The bandpass of the filter is located at the main frequency of the pattern that could be estimated using image profile samples as in [3]. The lower cut-off frequency (f_{low}) has to be chosen to reject the background information without impacting on the orientation while the upper cut-off frequency (f_{up}) to determine the amount of noise (sudden changes) that are to be cancelled. For our images the values of f_{low} and f_{up} have been empirically set to 0.1 and 0.17 (in terms of normalised frequency), respectively.

The filtered image contains the magnitude information for two classes, the background and the foreground (oriented pattern). In order to normalise the magnitude across the different classes and to separate them, the Otsu's algorithm [10] is applied. This algorithm provides a threshold to separate the information. By thresholding the image the corresponding binary image can be obtained. In Figure 1, both results of the statistical block normalisation (centre) and the frequency based normalisation (right) are shown.

B. Gradient based method

Following Kass and Witkin [9] and their notation, the first step is to calculate the image gradients in the x and y directions, $C_x(x, y)$ and $C_y(x, y)$, respectively. Different operators can be used to obtain the gradient information. Here, a Gaussian function with standard deviation σ_1 is used. These gradients can be combined to form the vector field $J(x, y)$ as

$$J(x, y) = C_x(x, y) + jC_y(x, y).$$

One cannot smooth the gradient vectors because vectors pointing in opposite directions would cancel each other. For that reason, the arguments of the elements of $J(x, y)$ are first doubled by means of squaring $J(x, y)$ and then three parameters are extracted from the square of $J(x, y)$: the imaginary part J_1, the real part J_2 and the gradient magnitude J_3, calculated as

$$J_1(x, y) = \Im[J(x, y)^2] = 2C_x(x, y)C_y(x, y),$$

$$J_2(x, y) = \Re[J(x, y)^2] = C_x^2(x, y) - C_y^2(x, y),$$

$$J_3(x, y) = |J(x, y)^2| = \sqrt{C_x^2(x, y) + C_y^2(x, y)},$$

respectively. The next step is to smooth the three considered parameters by convolving them with a smoothing function $W(x, y)$. In our case, a Gaussian function with standard deviation σ_2 is used. The use of this function is recommended for computational efficiency. The three smoothed parameters are then computed as follows

$$J_i^*(x, y) = J_i(x, y) * W(x, y), \quad i = 1, 2, 3.$$

The local orientation is then given by

$$\Phi(x, y) = \frac{\pi}{2} + \frac{1}{2}\tan^{-1}\left(\frac{J_1^*(x, y)}{J_2^*(x, y)}\right),$$

while the coherence is given by

$$\chi(x, y) = \frac{\sqrt{J_1^*(x, y)^2 + J_2^*(x, y)^2}}{J_3^*(x, y)}.$$
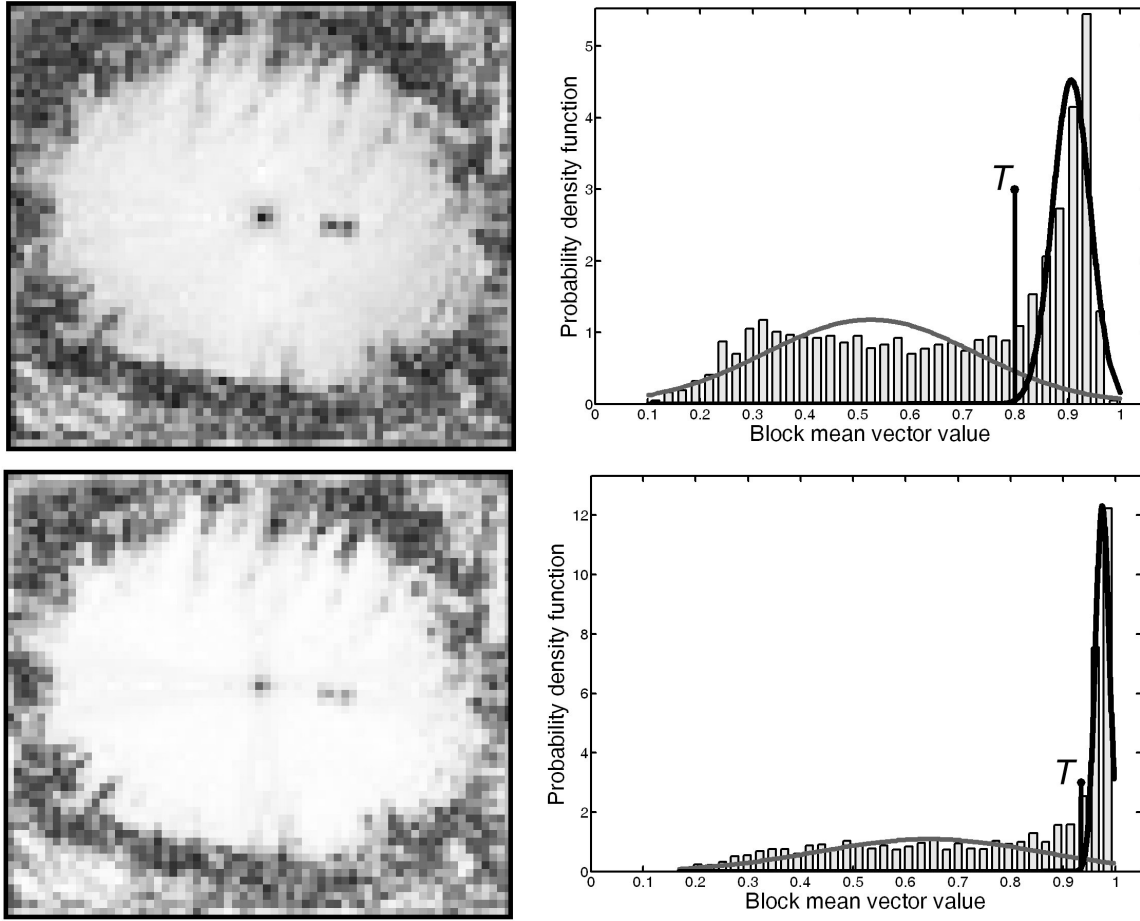
487

Fig. 2. Examples of coherence matrices and their distributions (together with the Gaussian mixture fits) using previously reported Gabor filter (top) and the proposed gradient based method (bottom).

Coherence, $\chi(x,y)$, has values between 0 for a weak coherence structure (anisotropic) and 1 for a strong coherence structure (isotropic).

The parameters σ_1 and σ_2 have to be selected depending on the image characteristics. The parameter σ_1 is used to separate the peak and the valleys in the original images, while σ_2 is responsible for smoothing the orientation results. Therefore, it is recommended that $\sigma_2 > \sigma_1$. For our application, the values have been set to $\sigma_1=1$ and $\sigma_2=3$. Examples of mean coherence matrices (see section *C* below) obtained with the previously reported Gabor filter method and the proposed gradient based method are shown in Figure 2 for the videokeratoscopic image from Figure 1 that was normalised using the frequency based technique.

C. Statistical analysis

For the sake of evaluation and comparison with a previously reported method, a statistical analysis is performed on the coherence matrix data in a similar way as in [3].

The coherence matrix is divided into non-overlapped blocks of 10×10 pixels. For each block, we calculate its sample mean, hence creating the mean-coherence matrix. By concatenating all the columns of this matrix we form the *mean coherence vector* on which further statistical analysis is performed. An estimator of the probability density function of this vector, such as the histogram, normally reveals a bimodal distribution in which the first mode represents the interference or anisotropic blocks of the image while the second represents the isotropic information in the image. In Figure 2, histograms of the mean-coherence vector with the two modes are clearly seen.

The probability density function of the mean coherence vector can be modeled as a Gaussian mixture

$$\phi(x[n];\epsilon) = (1-\epsilon)\phi_{\text{signal}}(X) + \epsilon\phi_{\text{noise}}(X),$$

where ϵ is the mixture parameter, which satisfies $0 < \epsilon < 1$, while ϕ_{signal} and ϕ_{noise} are the Gaussian probability density functions of the oriented and non-oriented blocks, respectively. An Expectation-Maximization algorithm is used to estimate the parameters of the Gaussian mixture [11], $\hat{\mu}_{\text{signal}}$, $\hat{\sigma}_{\text{signal}}$, $\hat{\mu}_{\text{noise}}$, and $\hat{\sigma}_{\text{noise}}$. Given these parameters, the estimates of the probability density function of noise $\hat{\phi}_{\text{noise}}(X)$ and that of the signal $\hat{\phi}_{\text{signal}}(X)$ can be evaluated as well as the detector
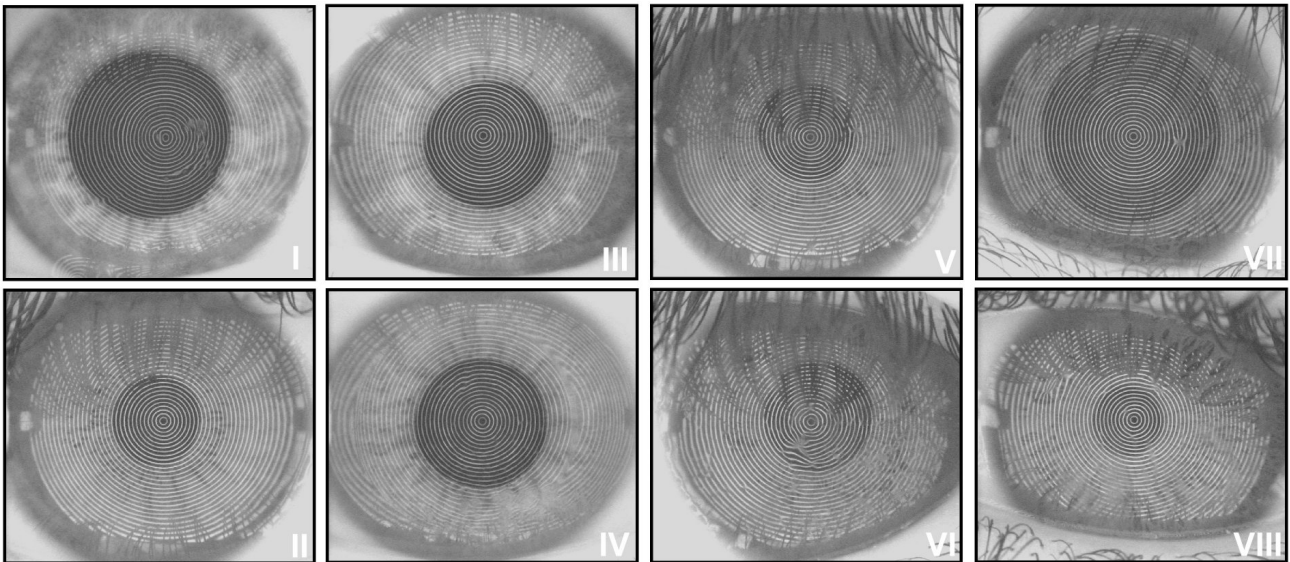
Fig. 3. Examples of videokeratoscopic images with different interference patterns.

characteristics [12] in terms of the probability of false alarm

$$P_{FA} = \int_T^1 \hat{\phi}_{\text{noise}}(X)dX,$$

and the probability of detection

$$P_D = \int_T^1 \hat{\phi}_{\text{signal}}(X)dX,$$

where T is the threshold point that distinguishes between the signal and interference. It is desirable that the values of the P_D are high and for this reason the threshold was chosen to be $T = \hat{\mu}_{\text{signal}} - 3\hat{\sigma}_{\text{signal}}$. This ensures that the values of P_D are close to 99.7%. Ideally the values of P_{FA}, which are used to evaluate the performance of the algorithm, should be small.

III. EXPERIMENTAL RESULTS

In order to evaluate the performance of the proposed technique we tested the algorithm on a number of real images. Here, a selection of representative cases is shown in Figure 3. To compare the current technique with the previously reported method each of the images was analysed with the different algorithms. First the image was normalised with the statistical block normalisation proposed in [3]. Then the normalised image was analysed with the Gaussian gradient-based and Gabor filter approaches. The same procedure was then repeated for the frequency normalised image.

Figure 2 shows the estimated coherence matrices and their distributions for the videokeratoscopic image from Figure 1. We note that the proposed gradient based method results in a more compact estimate of the probability density for the signal, hence separating it more from the noise than in the case of the Gabor filter based approach.

TABLE I
THE PROBABILITY OF FALSE ALARM (%) FOR THE EIGHT CONSIDERED VIDEOKERATOSCOPIC IMAGES.

Normalisation		Statistical	Frequency
Case	Gabor/Gradient	P_{FA}	P_{FA}
I	Gabor	6.95	3.89
	Gradient	4.41	2.85
II	Gabor	1.50	4.22
	Gradient	1.53	2.45
III	Gabor	6.46	4.81
	Gradient	6.33	3.48
IV	Gabor	10.10	6.87
	Gradient	7.22	4.62
V	Gabor	2.58	7.06
	Gradient	2.46	4.23
VI	Gabor	29.39	9.44
	Gradient	6.69	5.16
VII	Gabor	4.77	7.85
	Gradient	4.14	4.07
VIII	Gabor	6.49	3.49
	Gradient	13.25	2.40

A. Statistical Performance

Detailed results of statistical performance are given in Table I. The eight pattern cases are a representative sample of images with interference that can be encountered in videokeratoscopy. For each of the cases the probability of false alarm P_{FA} is provided for the four different conditions. Note that the probability of detection is set to 99.7% in all cases. The average improvement in P_{FA} using frequency based normalisation instead of statistical block normalisation was found to be negative for the Gabor filter (-25.5%) and positive for the gradient based method (11.4%). This suggests that the chosen normalisation algorithms are optimal for each of

489

TABLE II
THE AVERAGE CPU TIMES [SEC] FOR ALL PRESENTED CASES. TIMES
SHOWN INCLUDE BOTH THE NORMALISATION AND PATTERN ANALYSIS.

Normalisation		Statistical	Frequency
Case	Gabor/Gradient	Time	Time
All cases	Gabor	23.38±0.93	19.12±0.89
	Gradient	0.76±0.01	0.92±0.00

their approaches. However, comparing the Gabor filter based approach to that of the gradient based it is clear that the latter results in a lower P_{FA}. The average improvement is 6.9% for images normalised with statistical block technique and 36.7% for those normalised with frequency based technique.

B. Computational Efficiency

The average (± standard deviation) estimated CPU times for all considered methods for processing a single videokeratoscopic image are given in Table II. The results indicate that the gradient based approach is much more efficient in terms of computational effort than that based on the Gabor filter. While there is not much difference between the types of normalisation, the statistical block approach appears to be slightly faster. The algorithm was run on a Pentium IV(duo) at 1.86GHz.

IV. SUMMARY

Detecting interference patterns in videokeratoscopic images can be useful in corneal topography measurements in which the stability of tear film is not guaranteed (e.g., subjects with dry eyes) but not essential because an operator may ask the subject to blink several times to refresh the tear film and try to acquire a better image. However, in dynamic videokeratoscopy [7], pattern interference detection is a necessity.

We have proposed a novel method to detected and extract interferences form videokeratoscopic images. In the method we apply Gaussian gradient methods to a previously frequency-based normalised image and calculate image pattern coherence.

The results show significant improvement in terms of reduction of the probability of false alarm and low computational load with respect to a previously reported method [3]. The techniques proposed in this paper provide us with a computationally efficient tool that can be used to extract useful information from a videokeratoscopic image, assess its quality and be used in the future to analyse tear film surface quality.

REFERENCES

[1] T. Buehren, M. J. Collins, D. R. Iskander, B. Davis, and B. Lingelbach, "The stability of corneal topography in the post-blink interval," *Cornea*, vol. 20, no. 8, pp. 826–833, 2001.

[2] T. Buehren, B. J. Lee, M. J. Collins, and D. R. Iskander, "Ocular microfluctuations and videokeratoscopy," *Cornea*, vol 21, no. 4, pp. 346–351, 2002.

[3] D. Alonso-Caneiro, D. R. Iskander, and M. J. Collins, "Estimating corneal surface topography in videokeratoscopy in the presence of strong interference," *IEEE Transactions on Biomedical Engineering*, d.o.i. 10.1109/TBME.2008.923766.

[4] J. Németh, B. Erdélyi, B. Csákány, P. Gáspár, *et al.*, "High-speed videotopographic measurement of tear film build-up time," *Investigative Ophthalmology and Visual Science*, vol. 43, no. 6, pp. 1783–1790, 2002.

[5] R. Montés-Micó, J. L. Alió, G. Muñoz, and W. N. Charman, "Temporal changes in optical quality of air-tear film interface at anterior cornea after blink," *Investigative Ophthalmology and Visual Science*, vol. 45, no. 6, pp. 1752–1757, 2004.

[6] T. Goto, X. Zheng, S. Klyce, H. Kataoka, *et al.*, "Evaluation of the tear film stability after laser in situ keratomileusis using the tear film stability analysis system," *American Journal of Ophthalmology*, vol. 137, no. 1, pp. 116–120, 2004

[7] D. R. Iskander, and M. J. Collins, "Applications of high-speed videokeratoscopy," *Clinical and Experimental Optometry*, vol. 88, no. 4, pp. 223–231, 2005.

[8] D. R. Iskander, M. J. Collins, and B. Davis, "Evaluating tear film stability in the human eye with high-speed videokeratoscopy," *IEEE Transactions on Biomedical Engineering*, vol. 52, no. 11, pp. 1939–1949, 2005.

[9] M. Kass, and A. Witkin, "Analyzing oriented patterns," *Computer Vision, Graphics, and Image Processing*, vol. 37, no. 3, pp. 362–385, 1987.

[10] N. Otsu, "A threshold selection method from gray-level histograms," *IEEE Transactions on Systems, Man and Cybernetics*, vol. 9, no. 1, pp. 62–66, 1979.

[11] T. K. Moon, "The expectation-maximization algorithm," *IEEE Signal Processing Magazine*, vol. 13, no. 6, pp. 47–60, 1996.

[12] H. L. Van Trees, "Detection, Estimation and Modulation Theory. Part I," *John Wiley & Sons, New York*, pp. 720, 1968.